

Arrangement of La and vacancies in $\text{La}_{2/3}\text{TiO}_3$ predicted by first-principles density functional calculation with cluster expansion and Monte Carlo simulation

Masanobu NAKAYAMA,^{*,**,†} Atsushi SHIRASAWA^{***} and Toshiya SAITO^{***}

^{*}Department of Applied Chemistry, Tokyo Institute of Technology, Ookayama, Meguro-ku, Tokyo 152-8552

^{**}Department of Materials Science and Engineering, Nagoya Institute of Technology, Gokiso-cho, Syowa-ku, Nagoya-shi, Aichi 466-8555

^{***}Battery Research Division, Toyota Motor Corporation, 1200, Mishuku, Susono, Shizuoka 410-1193

High ionic conductivity of lithium in $\text{Li}_x\text{La}_{(2-x)/3}\text{TiO}_3$ with A-site deficient type perovskite structure has attracted considerable attention owing to both the range of practical usage (e.g., all-ceramics Li secondary batteries) and the fundamental fascination of fast lithium ion transport in crystalline solids. In present paper, we investigated the arrangement of La and vacancies in $\text{La}_{2/3}\text{TiO}_3$ by means of first-principles computations combined with cluster expansion approach, since it has caused a difficulty of atomistic level discussion due to numerous freedoms of configuration. The computational results predicted the alternate La concentrated and diluted layers stacking along *c*-axis, which agreed with the previous structural analyses. In addition, La cluster formation within *ab* plane is indicated. Using predicted La/vacancy arrangement, we demonstrated to calculate the Li migration path and energy profiles during Li jump by nudged elastic band method, which showed diagonal pathways to avoid passing A-site center.

©2009 The Ceramic Society of Japan. All rights reserved.

Key words : Li ion conductor, First-principles calculation, Cluster expansion, La/vacancy arrangement

[Received April 17, 2009; Accepted June 18, 2009]

1. Introduction

Development of inorganic materials with high Li^+ conductivity is vital to realize all-ceramics Li secondary batteries. Among them, A-site deficient perovskite oxides containing Li^+ have been received much attention due to their considerable Li^+ conductivity. For example, $\text{Li}_x\text{La}_{(2-x)/3}\text{TiO}_3$ (LLTO) shows relatively high ionic conductivity of Li in the order of 10^{-3} S cm^{-1} at room temperature.^{1)–3)} In this system, Li, La ions and vacancies are distributed at perovskite A-site, while Ti ions reside in perovskite B-site, and Li ions migrate between two A-sites through the vacancy. (See following section which describes detailed structural description.)

There have been numerous reports on the exploration of ionic conductivity and/or crystal structure of these perovskite oxides, and these studies revealed a strong relationship between ionic conductivity and crystal structure.^{4)–18)} For example, activation energy for Li^+ conduction decreases with the expansion of the lattice by doping alkaline earth metals.⁵⁾ Extended X-ray absorption fine structure (EXAFS) measurements suggested that local distortion of lattice caused a decrease of the ionic conductivity of Li in $\text{Li}_x\text{La}_{(1-x)/3}\text{NbO}_3$ system.¹⁹⁾ Therefore, detailed structural description would give an insight into proper material design for high ionic conductivity. In this respect, *ab initio* density functional (DF) calculation is one of the most promising ways to obtain the knowledge on local atomic arrangements and its energetic relationship. For example, Catti has been reported recently the local structure of $\text{Li}_{1/8}\text{La}_{5/8}\text{TiO}_3$ by *ab initio* DF calculations.²⁰⁾ The computational results showed (1) the formation of

alternate stacking of La-poor and La-rich layer in perovskite A-sites along *c*-axis, (2) anti-phase tilting of BO_6 octahedron due to mixed La-Li local composition of the layers, (3) Li ions distribution at peripheral sites around A-site center, and so on. Despite above successes by *ab initio* computation, fundamental difficulties still remains for structural modeling by computation due to the fact that the degree of configurational freedom at perovskite A-sites (or, conceivable arrangements of La/Li/vacancies) is too numerous.

To overcome this problem, *ab initio* DF prediction of favorite La/vacancy (binary) arrangements in $\text{La}_{2/3}\text{TiO}_3$ has been carried out in present study with the aid of cluster expansion and Monte Carlo simulation.^{21,22)} Note that the present study is the first step on the way to predict the Li/La/vacancy (ternary) configuration at arbitrary lithium composition. However, the location of Li ions is largely deviate from the center of A-sites, causing difficulty to apply cluster expansion method directly. (This phenomenon will be mentioned in the results section.) Thus, we simulated the extreme case of $\text{La}_{2/3}\text{TiO}_3$ where Li ions are absent. The results would be useful to understand ionic conductivity in dilute regime of Li concentration in LLTO. For a demonstration purpose, nudged elastic band method (NEB)²³⁾ was used to simulate the Li^+ jumps in the lattice using preferable La/vacancy local arrangement of simulated $\text{La}_{2/3}\text{TiO}_3$.^{*,24)}

2. Structure description

The crystal structure of $\text{Li}_x\text{La}_{(2-x)/3}\text{TiO}_3$ has been studied by many researchers as mentioned above. **Figure 1** shows the crys-

* $\text{La}_{2/3}\text{TiO}_3$ ($y = 0$) usually contained impurity phase under air atmosphere or oxygen vacancy with partial reduction of Ti ions.; See such as ref. 24.

† Corresponding author: M. Nakayama; E-mail: masanobu@nitech.ac.jp

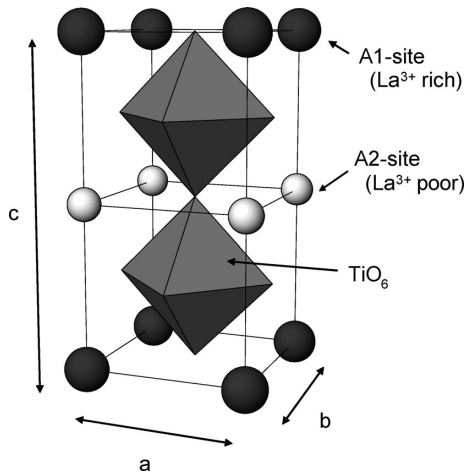


Fig. 1. Crystal structure of $\text{La}_{2/3}\text{TiO}_3$ based on ref. 9.

tal structure of $\text{Li}_x\text{La}_{(2-x)/3}\text{TiO}_3$ based on the ref. 9. La ions, Li ions, and vacancies are distributed in perovskite A-site and ordered within alternate (001) planes doubling the c-parameter of the primitive perovskite cell of ABO_3 , where one of the (001) planes possess larger amount of La ions (La-rich layer) than the other planes (La-poor layers). In addition, the structure was lead to slightly distorted orthorhombic lattice with parameters $a-a_p$, $b-a_p$, $c-2a_p$ (a_p refers to the cubic-perovskite type unit cell: Hereinafter, a_p was referred as the ‘averaged perovskite parameter’). It was observed that the crystal symmetry changed from orthorhombic to tetragonal and then to pseudo-cubic with increasing the lithium content in the perovskite structure of $\text{Li}_x\text{La}_{(2-x)/3}\text{TiO}_3$. Such a structural change was ascribed to the disordering of A-site cations.⁹⁾

3. Computational method

The basic approach of present investigation can be described in the ref. 22 and divided into three steps. In the first step, *ab initio* DF calculations of $\text{La}_{2/3}\text{TiO}_3$ were driven to obtain total energy at various configurations of La ions and vacancies. Vienna *ab initio* simulation package (VASP)^{25),26)} was utilized with generalized gradient approximation (GGA)²⁷⁾ and with the projector-augmented wave (PAW) method.²⁸⁾ Relaxation of crystal structure was allowed and the final energies of the optimized structural geometries were recalculated so as to correct for changes in the plane-wave basis during relaxation. The detailed conditions of DF calculations are along with previous report for $\text{Li}_x\text{La}_{1/3}\text{NbO}_3$.²⁹⁾

In the second step, a subset of the calculated ~50 total energies corresponding to different La/vacancy arrangements within the TiO_3 framework was converted to effective cluster interactions (ECI) to estimate the total energy E of the crystal with arbitrary La/vacancy arrangement rapidly and precisely. This can be done by a generalized lattice model base on the cluster expansion formalism.²¹⁾⁻²²⁾ In the cluster expansion formalism, occupation variables σ_i are assigned to each La/vacancy site i within the host framework. σ_i is +1 if a La ion occupies at site i , and σ_i is -1 if a vacancy sits the site i . The total energy E with arbitrary La/vacancy arrangement can be expressed as the summation of polynomial ϕ_α of these occupation variables:

$$E = \sum_{\alpha} V_{\alpha} \cdot \phi_{\alpha} \quad (1)$$

where

$$\phi_{\alpha} = \prod_{i \in \alpha} \sigma_i \quad (2)$$

which corresponds to a product of occupation variables associated with La sites belonging to the cluster α . The clusters α consist of pair clusters of nearest neighbor, next nearest neighbor, and so on, and triplet clusters in this study. The coefficients V_{α} are ECI as mentioned above and are the constants determined by the fitting to first-principles total energies. Note that the formalism is exactly the same as Ising model if one uses within the pair cluster.

The third step is MC calculation using fitted ECI values which enables us to determine total energy for any La/vacancy configuration from Eqs. (1) and (2). Canonical MC approach was adopted for the energetic and structural analyses, such as free energy and site occupancy variation with temperature, etc. Note that ECI values used in the Monte Carlo simulation are determined by referring the *ab initio* total energy considering structural relaxation, so that obtained energies by Monte Carlo simulation reflect the local structural information, such as fractional coordinates change for La, Ti, O owing to La/vacancy configurations. However, the concrete values of fractional coordinates cannot be obtained by Monte Carlo in this case, since the ECI only give energy values for system. Supercell constructed by $12 \times 12 \times 12$ expansion of the cubic unitcell (ABO_3) with total 1728 sites for La/vacancy was used in this study, since the obtained energy were minimum among the other systems with different supercell size. This is due to a problem of Monte Carlo convergence in $\text{La}_{2/3}\text{TiO}_3$ system where twin formation was indicated in the simulation using larger supercell (we will discuss later part of this paper). The temperature was varied and cycled twice ranging from 100 to 2000 K unless specially mentioned. ATAT program package was used for the cluster expansion approach and MC simulations.^{30),31)}

The nudged elastic band (NEB) method was used to investigate the minimum energy pathways of the lithium ion hopping from one lattice position to adjacent sites. First, the two point configurations (initial and end point) and the corresponding total energies were calculated by specifying the location of a vacancy at the two potential minima. In this computation, the internal atomic positions in the cell were relaxed without changing the lattice parameter, as mentioned above. Then intermediate configurations were generated by linear interpolation between the initial and end points. Finally, the intermediate configurations were relaxed under the constraint that the ions were connected by springs to keep the ions equidistant from neighbouring configurations during the relaxation. Details of the NEB method are described in ref. 23.

4. Results and discussion

Figure 2 presents the total energies for 29 types of La/vacancy configurations calculated by first-principles DF (E_{DF} , horizontal axis) and cluster expansion formalism (Eqs.(1)–(2)) with fitted ECI values (E_{ECI} , vertical axis). Note that the lowest (most stable) energy for E_{DF} is set as zero. As seen in the figure, E_{ECI} by cluster expansion formalism showed good accordance with obtained E_{DF} for all the plots (from 29 configurations), and the root mean square error is sufficiently small. Thus, we confirmed that the cluster expansion formalism (Eqs.(1)–(2)) can mimic the calculated total energy by *ab initio* DF method for $\text{La}_{2/3}\text{TiO}_3$ system.

Figure 3 plots the fitted ECI values as a function of interaction distance which was normalized by averaged perovskite parameter a_p . The open circles are for the pair cluster (two body interaction), and the cross symbol represent for the triplet clusters. In

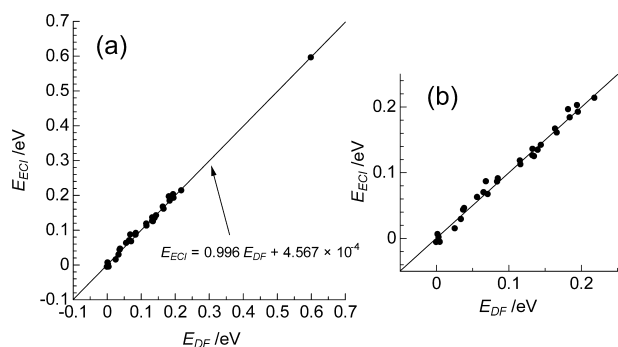


Fig. 2. Comparison of the calculated total energies obtained by DF calculation (E_{DF}) and fitting using cluster expansion approach (E_{ECI}). The lowest energy among 29 structures are set as zero for E_{DF} . Magnification of the plots around 0 eV is shown in panel (b). Least square fit results using linear function was also displayed as solid line. (Root mean square error of fitted line is 6.98×10^{-3} .)

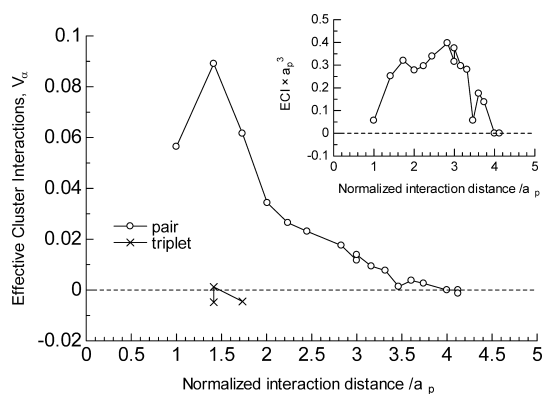


Fig. 3. Variation of the effective cluster interactions (ECI) versus interaction distance. Open circles and cross symbols indicate the pair and triplet cluster. Interaction distances of clusters are normalized by averaged perovskite lattice parameter a_p . Inset plots the products of ECI for pair cluster and perovskite parameter cubed ($ECI \times a_p^3$) as a function of normalized interaction distance.

present study, ECIs from 16 pair clusters, and 3 triplet clusters were used to reproduce the DF total energy. All the ECI values of pair clusters were positive, indicating the La–La (and vacancy–vacancy) interactions are repulsive. One can see that this tendency weakened as the interaction distance increased, and the ECI became almost zero (no interaction) beyond 3.5 Å. However, numbers of the clusters in lattice are increased as interaction distance, so that it is difficult to conclude shortly whether the long-range interaction was negligible. To estimate roughly the effect of increased number of interaction pairs, the product of ECI and normalized interaction distance cubed ($ECI \times a_p^3$) was plotted as a function of normalized interaction distance. The results indicated the pair cluster interaction will be decreases with distance at least more than $\sim 3 a_p$, and ECI reached zero around $\sim 4 a_p$. Hence, the cut-off distance for pair interaction is small enough in this computation.

Figure 4 shows the variation of the energy and cell volumes for 29 configurations of $La_{2/3}TiO_3$ obtained by DF calculations. The energies did not show obvious correlation with cell volumes, so that we concluded that the changes in energy of the system related to arrangement of La/vacancies rather than volume change.

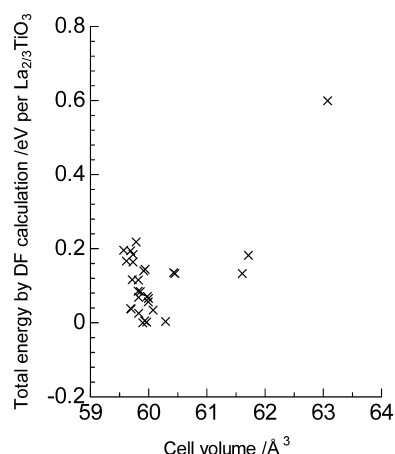


Fig. 4. Comparison of total energy and cell volumes by DF calculation for $La_{2/3}TiO_3$ with 29 configurations.

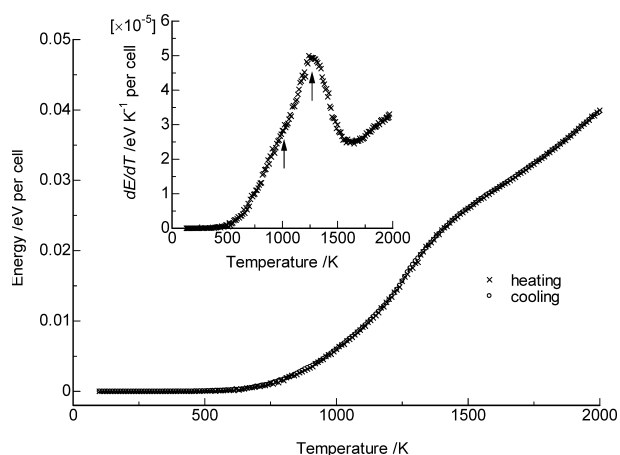


Fig. 5. Variation of the energy as a function of temperature in $La_{2/3}TiO_3$ calculated by canonical Monte Carlo method. Cross and open circle symbols indicate energy variation with heating and cooling process, respectively. Inset of the figure displays the derivative of energy against temperature (it corresponds to heat capacity). Arrows point the phase transition.

Figure 5 represents the variation of energy obtained by canonical MC as a function of temperature. Inset of the figure shows the derivative of energy against temperature (which is heat capacity at constant volume, or entropy change), showing at least two phase transitions from 100 to 2000 K. Apparent phase transition can be seen around 1250 K (see arrow in Fig. 5), and the other one was indicated as faint hump appeared around 1000 K. These phase transition behaviors would not ascribed to the first-order phase transition, since the energy profiles showed perfect agreement for heating and cooling process and the derivative curves are continuous function.

Before investigating origin of the phase transitions, the most stable La/vacancy array was analyzed using structural snapshot of Monte Carlo result at 100 K as shown in **Fig. 6**. At sufficiently low temperature (100 K), La ions (and vacancies) ordered within alternate (001) planes, doubling the c -parameter of the primitive perovskite cell of $La_{2/3}TiO_3$. One of the planes is fully occupied by La ions (La-rich plane), and remaining 1/6 La ions are located in the other plane (La-poor plane). This structural feature of alternate stacking of La-rich and –poor planes agreed well with

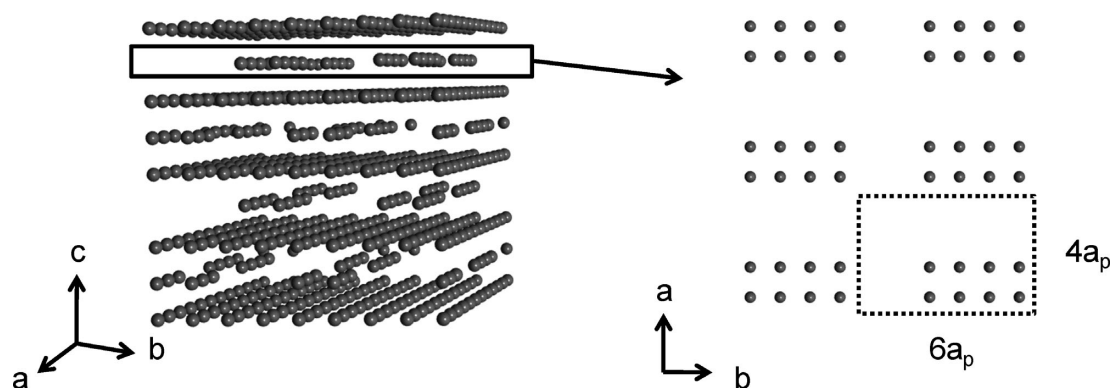


Fig. 6. Part of the snapshot of La/vacancy arrangement in $\text{La}_{2/3}\text{TiO}_3$ at 100 K obtained by canonical Monte Carlo simulation. Right panel showed two dimensional La/vacancy array in one of the a - b plane as shown in figure.

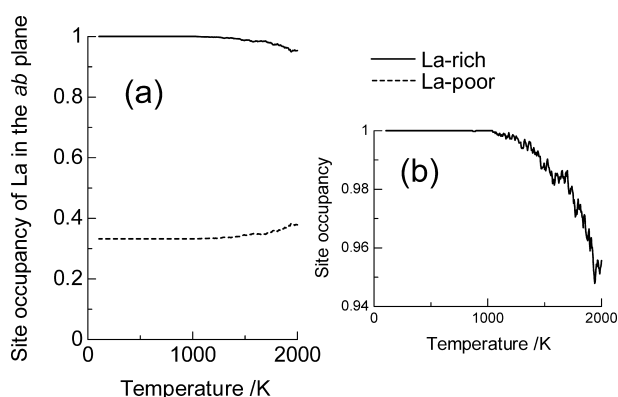


Fig. 7. Temperature dependence of the variation of the site occupancy of La ions in the ab plane of $\text{La}_{2/3}\text{TiO}_3$. (Panel (b) is magnification of panel (a).)

experimental analyses reported previously.^{9)–14)} In addition, La ions and vacancies ordered within La-poor planes in the direction of ab -axis as shown in the right panel of Fig. 6. In this structure, eight La ions were formed 2×4 rectangular-shape clusters arranging ordered manner with keeping two-vacancy-site intervals, resulting in $4a_p \times 6a_p$ periodic unit in the ab -planes. These La-clusters alternately stacked along c -axis to keep distant each other. Such a ordering along ab planes may be one of the reasons of the orthorhombic distortion mentioned in previous reports.^{12),14),16),18)} Hence, we inferred that the phase transitions appeared in Fig. 5 may relate to (partial) disordering of such La/vacancy ordered arrays in the lattice.

Figure 7 displays the variation of the site occupancy of La ions for La-rich and La-poor planes of $\text{La}_{2/3}\text{TiO}_3$ with temperature. As shown in Fig. 6, site occupancy of La ions at 100 K is unity (full occupation) and $1/3$ in La-rich and La-poor planes, respectively. This ordered array of alternate stacking along c -axis began to break around 1000 K. Thus, this break would relate to the hump of the heat capacity simulated around 1000 K in Fig. 5. Since the variation of the site occupancy showed continuous change, so that second-order phase transition occurred as mentioned before. Note that the ordered nature remains strongly even at 2000 K, because the site occupancies in La-rich and La-poor planes are still apart.

The coordination number (CN) of nearest neighbor (NN) interactions between La and La in the La-poor planes is plotted in **Fig. 8**. The perovskite A-sites are neighbored with 4 La/

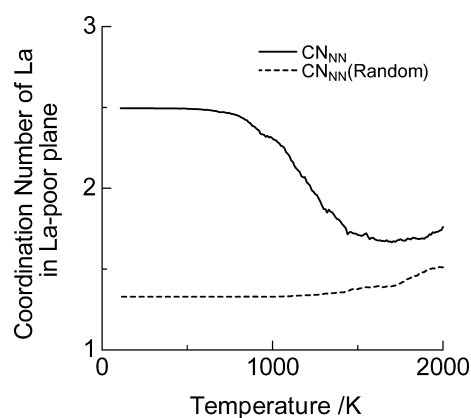


Fig. 8. Temperature dependence of the variation of the coordination number (CN) of La ions in La-poor plane of $\text{La}_{2/3}\text{TiO}_3$. Solid and hatched lines indicate the result of MC simulation and expectation based on random arrangement of La/vacancy at La-poor plane, respectively.

vacancy sites in the two dimensional La-poor plane. Solid line and hatched line in Fig. 8 indicate simulated CN of NN interactions (CN_{NN}) and expected ones where random La ion distribution was assumed ($\text{CN}_{\text{NN}}(\text{Random})$) in La-poor plane. (The slight increase of the $\text{CN}_{\text{NN}}(\text{Random})$ above 1000 K owes to increasing of site occupancy as shown in Fig. 7.) The calculated CN_{NN} was always larger than the $\text{CN}_{\text{NN}}(\text{Random})$, so that the ordered nature of La/vacancy arrangement in La-poor plane was kept ranging from 100–2000 K. At low temperature region, the CN_{NN} was 2.5 which corresponds to formation of 2×4 rectangular La cluster (Fig. 8). This cluster formation began to break around 500–800 K, and the CN_{NN} decrease sharply in the temperature range of 1000–1400 K. The latter phenomena agreed with the peak of heat capacity at ~ 1250 K (Fig. 5). Finally, the CN_{NN} finally reached stable value above ~ 1400 K, indicating a formation of another (global or local) ordering of La/vacancy arrays.

To investigate the La/vacancy array in La-poor plane at high temperature region, the snapshot of MC calculations at 2000 K is shown in **Fig. 9**. The results indicated collapse of 2×4 rectangular La-cluster and no long-range superstructure formation. (It seems random arrangement of La/vacancy at first glance.) However, La ions may prefer to array liner manner along a (or b) axis rather than to array diagonal directions in Fig. 9 as can be expected from a larger CN_{NN} than $\text{CN}_{\text{NN}}(\text{random})$. Further study based on quantitative analyses is needed in order to capture

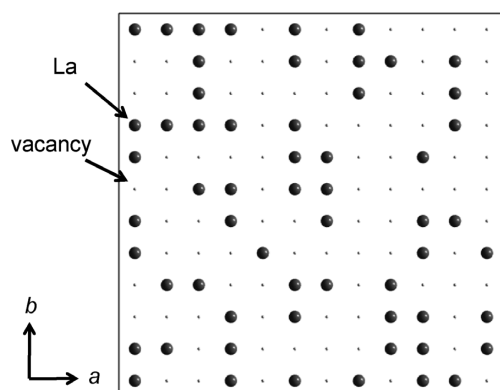


Fig. 9. Snapshot of La/vacancy array in La-poor plane at 2000 K.

the structural feature of high temperature region.

One of the problems of present Monte Carlo simulation is the use of the small supercell size ($12 \times 12 \times 12$) as mentioned before. This small supercell was suited to analyze short-range structure, but difficult to discuss long-range interactions. Our tentative study using large scale supercell showed twin formation in the supercell, and we expect the twin formation is essential in this structure. However, this behavior strongly depended on the size of supercell, so that analyses for the formation of twins and long-range ordering behavior using large supercell are now in progress. (Thus, above obtained results may reflect the energetics of point defect formations inside single crystal domains.)

Heretofore, the preferred La/vacancy arrangement was discussed using Monte Carlo simulation, and we revealed several structural features at low temperature, such as alternate stacking of La-rich and La-poor planes and La clustering in La-poor plane, as shown in Fig. 6. These structural features may be important and cause an effect strongly for simulating Li ion conduction at diluted Li concentration regime in $\text{Li}_x\text{La}_{(2-x)/3}\text{TiO}_3$ around room temperature (where Li ion conductor is expected to be mainly used for application purpose). Thus, NEB method was adopted to demonstrate the Li ion jumps between the lattices as shown in Fig. 10. Because of the large size periodicity of predicted superstructure shown in Fig. 6, part of the cell was taken out with $3 \times 3 \times 2$ cubic-perovskite units for *ab initio* DF calculations which mimic roughly the features of La/vacancy arrays. One Li ion was put at the center of A-site and simulated the jump path and jump energy profile using NEB. The number of electrons was adjusted to be the total valence state of the cell which was composed of Li^+ , La^{3+} , Ti^{4+} and O^{2-} . A jellium background was used to neutralize the lattice. The results of NEB calculations are summarized in Fig. 11. The Li ion was stabilized not at the center of perovskite A-site, but at the center of two adjacent A-sites (3c site in $Pm3m$ cubic-perovskite symmetry). Li ions jumped along diagonal directions of *ab* axis, and reached an energy maximum at vicinity of A-site center. The diffusion path of Li ions showed agreement with recent neutron diffraction study by Yashima et al.,¹⁷⁾ suggesting the validity of simulated cell in Fig. 10. The energy profiles in Fig. 11(b) show two potential minima at position 0 and 4 corresponding to 3c sites in $Pm3m$ symmetry. These stable sites are, however, the smallest in spatial size along diffusion path, so that the attractive Coulombic interactions between anion and diffusive Li^+ may be dominant. In addition, relatively larger potential energy in position 4 than in position 0 would be due to the repulsive Coulombic interaction between Li^+ and La^{3+} which locate neighboring cation sites for

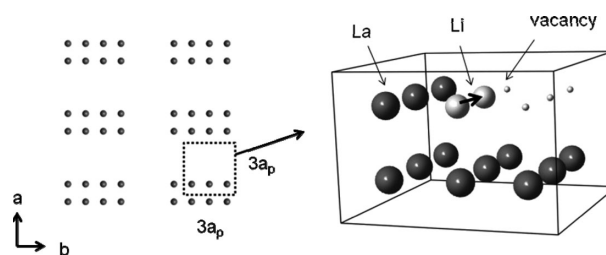


Fig. 10. Structure model for the computation of Li jump in $\text{La}_{2/3}\text{TiO}_3$ structure by NEB method. For viewing purpose, Ti and O ions were omitted in this figure.

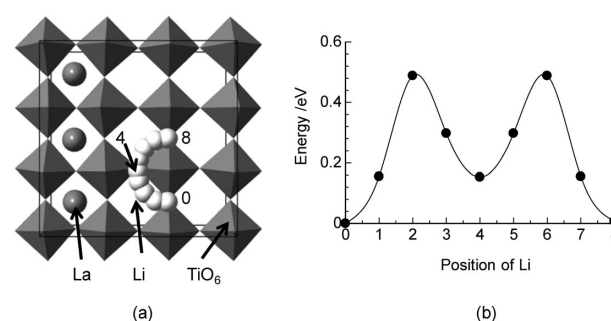


Fig. 11. (a) Li jump path and (b) corresponding energy profile predicted by *ab initio* DF and NEB calculations. The numbers of Li ions shown in panel (a) refer to the position of Li (horizontal axis) in the graph (b).

Li^+ at position 4. In quantitative aspect, the activation energy was predicted around ~ 0.5 eV which was relatively larger than the experimental results (~ 0.3 eV).¹⁾⁻⁴⁾ Hence, we infer the other factors that reduce energy barrier between lattices, such as the cooperative two Li ions jump mechanism or importance of defect species in the cell.

5. Conclusion

In present paper, La/vacancy configurations in $\text{La}_{2/3}\text{TiO}_3$ structure were simulated as a function of temperature using *ab initio* DF calculations combined with cluster expansion and Monte Carlo simulation. The results are summarized as below.

Cluster expansion formalism can mimic the total energy by *ab initio* DF calculation with sufficient quality.

La-rich and La-poor planes were stacked alternately perpendicular to *c*-axis, which agreed well with the previous experimental results.

La cluster formation with 2×4 rectangular shapes was indicated in La-poor plane at low temperature regime, and this structural feature was broken at the temperature higher than phase transition.

NEB calculation indicated that Li ions located at the middle of neighboring A-sites, and activation position located around vicinity of A-sites center.

These results are the starting step for understanding Li ionic conduction behavior in $\text{Li}_x\text{La}_{(2-x)/3}\text{TiO}_3$ structure, and further study such as modeling larger Monte Carlo cell and detailed structural analyses for NEB results are now in progress.

Acknowledgement This work was partly supported by the Grant-in-Aid for Young Scientists (No. 20760450) from The Ministry of Education, Cultures, Sports, Science and Technology, Japan. Figures of crystal structure were drawn with VESTA.³²⁾

References

- 1) A. G. Belous, G. N. Novitskaya, S. V. Polyanskaya and Y. I. Gornikov, *Izvestiya Akademii Nauk SSSR, Neorg. Mater.*, **23**, 412–415 (1987).
- 2) Y. Inaguma, L. Chen, M. Itoh, T. Nakamura, T. Uchida, H. Ikuta and M. Wakihara, *Solid State Commun.*, **86**, 689–693 (1993).
- 3) H. Kawai and J. Kuwano, *J. Electrochem. Soc.*, **141**, L78–79 (1994).
- 4) S. Stramare, V. Thangadurai and W. Weppner, *Chem. Mater.*, **15**, 3974–3990 (2003).
- 5) Y. Inaguma, L. Chen, M. Itoh and T. Nakamura, *Solid State Ionics*, **70/71**, 196–202 (1994).
- 6) M. Itoh, Y. Inaguma, W. H. Jung, L. Chen and T. Nakamura, *Solid State Ionics*, **70/71**, 203–207 (1994).
- 7) Y. Harada, T. Ishigaki, M. Kawai and J. Kuwano, *Solid State Ionics*, **108**, 407–413 (1998).
- 8) J. A. Alonso, J. Sanz, J. Santamaria, C. León, A. Varez and M. T. Fernández-Díaz, *Angew. Chem. Int. Ed.*, **39**, 619–621 (2000).
- 9) C.-H. Chen and K. Amine, *Solid State Ionics*, **144**, 51–57 (2001).
- 10) J. Sanz, J. A. Alonso, A. Varez and M. T. Fernández-Díaz, *J. Chem. Soc., Dalton Trans.*, 1406–1408 (2002).
- 11) O. Bohnké, H. Duroy, J.-L. Fourquet, S. Ronchetti and D. Mazza, *Solid State Ionics*, **149**, 217–226 (2002).
- 12) Y. Inaguma, T. Katsumata, M. Itoh and Y. Morii, *J. Solid State Chem.*, **166**, 67–72 (2002).
- 13) D. Mazza, S. Ronchetti, O. Bohnké, H. Duroy and J.-L. Fourquet, *Solid State Ionics*, **149**, 81–88 (2003).
- 14) J. Sanz, A. Varez, J. A. Alonso and M. T. Fernández-Díaz, *J. Solid State Chem.*, **177**, 1157–1164 (2004).
- 15) S. Garcia-Martin, M. A. Alario-Franco, H. Ehrenberg, J. Rodriguez-Carvajal and U. Amador, *J. Am. Chem. Soc.*, **126**, 3587 (2004).
- 16) A. Varez, M. T. Fernández-Díaz, J. A. Alonso and J. Sanz, *Chem. Mater.*, **17**, 2404 (2005).
- 17) M. Yashima, M. Itoh, Y. Inaguma and Y. Morii, *J. Am. Chem. Soc.*, **127**, 3491–3495 (2005).
- 18) Y. Inaguma, T. Katsumata, M. Itoh, Y. Morii and T. Tsurui, *Solid State Ionics*, **177**, 3037–3044 (2006).
- 19) M. Nakayama, H. Ikuta, Y. Uchimoto and M. Wakihara, *Appl. Phys. Lett.*, **84**, 4227–4229 (2004).
- 20) M. Catti, *Chem. Mater.*, **19**, 3963–3972 (2007).
- 21) D. De Fontaine, *Solid State Phys.*, **47**, 33–176 (1994).
- 22) G. Ceder, A. van der Ven, C. Marianetti and D. Morgan, *Modelling Simul., Mater. Sci. Engl.*, **8**, 311–321 (2000).
- 23) H. Jonsson, G. Mills and K. M. Jacobsen, in “Classical and Quantum Dynamics in Condensed Phase Simulations,” Ed. by B. J. Berne, G. Ciccotti, D. F. Coker, World Scientific, Singapore (1998).
- 24) M. Nakayama, T. Usui, Y. Uchimoto, M. Wakihara and M. Yamamoto, *J. Phys. Chem. B*, **109**, 4135–4143 (2005).
- 25) G. Kresse and J. Furthmüller, *Phys. Rev. B*, **54**, 11169–11186 (1996).
- 26) G. Kresse and J. Furthmüller, *Comput. Mater. Sci.*, **6**, 15–50 (1996).
- 27) J. P. Perdew, K. Burke and M. Ernzerhof, *Phys. Rev. Lett.*, **77**, 3865–3868 (1996).
- 28) P. E. Blöchl, *Phys. Rev. B*, **50**, 17953–17979 (1994).
- 29) M. Nakayama, J. Shirakawa and M. Wakihara, *Solid State Ionics*, **177**, 1259–1266 (2006).
- 30) A. Van de Walle, M. Asta and G. Ceder, *Calphad*, **26**, 539–553 (2002).
- 31) A. Van de Walle, *Calphad*, in press (2008) Doi:10.1016/j.calphad.2008.12.005
- 32) K. Momma and F. Izumi, *J. Appl. Crystallogr.*, **41**, 653–658 (2008).